

SDSS J1254+0846: A BINARY QUASAR CAUGHT IN THE ACT OF MERGING

PAUL J. GREEN^{1,6}, ADAM D. MYERS^{2,6}, WAYNE A. BARKHOUSE^{3,6}, JOHN S. MULCHAHEY⁴, VARDHA N. BENNETT⁵,
THOMAS J. COX^{1,4}, AND THOMAS L. ALDCROFT¹

¹ Harvard-Smithsonian Center for Astrophysics, 60 Garden Street, Cambridge, MA 02138, USA; pgreen@cfa.harvard.edu

² Department of Astronomy, University of Illinois at Urbana-Champaign, 1002 West Green Street, Urbana, IL 61801-3080, USA

³ Department of Physics and Astrophysics, University of North Dakota, Grand Forks, ND 58202, USA

⁴ The Observatories of the Carnegie Institution for Science, 813 Santa Barbara Street, Pasadena, CA 91101, USA

⁵ Department of Physics, University of California, Santa Barbara, CA 93106, USA

Received 2009 October 21; accepted 2010 January 12; published 2010 February 1

ABSTRACT

We present the first luminous, spatially resolved binary quasar that clearly inhabits an ongoing galaxy merger. SDSS J125455.09+084653.9 and SDSS J125454.87+084652.1 (SDSS J1254+0846 hereafter) are two luminous $z = 0.44$ radio-quiet quasars, with a radial velocity difference of just 215 km s^{-1} , separated on the sky by 21 kpc in a disturbed host galaxy merger showing obvious tidal tails. The pair was targeted as part of a complete sample of binary quasar candidates with small transverse separations drawn from SDSS DR6 photometry. We present follow-up optical imaging which shows broad, symmetrical tidal arm features spanning some 75 kpc at the quasars' redshift. Previously, the triggering of two quasars during a merger had only been hypothesized but our observations provide strong evidence of such an event. SDSS J1254+0846, as a face-on, pre-coalescence merger hosting two luminous quasars separated by a few dozen kpc, provides a unique opportunity to probe quasar activity in an *ongoing* gas-rich merger. Numerical modeling suggests that the system consists of two massive disk galaxies prograde to their mutual orbit, caught during the first passage of an active merger. This demonstrates rapid black hole growth during the early stages of a merger between galaxies with pre-existing bulges. Neither of the two luminous nuclei show significant intrinsic absorption by gas or dust in our optical or X-ray observations, illustrating that not all merging quasars will be in an obscured, ultraluminous phase. We find that the Eddington ratio for the fainter component B is rather normal, while for the A component L/L_{Edd} is quite ($>3\sigma$) high compared to quasars of similar luminosity and redshift, possibly evidence for strong merger-triggered accretion. More such mergers should be identifiable at higher redshifts using binary quasars as tracers.

Key words: black hole physics – galaxies: active – galaxies: interactions – galaxies: nuclei – quasars: emission lines

1. INTRODUCTION

The origin, growth, and evolution of massive galaxies, and the supermassive black holes (SMBHs) that they host, represent a prime field of study in modern astrophysics. We now know that galaxies regularly interact and merge (Toomre & Toomre 1972), and that SMBH resides in the centers of most, if not all galaxies (e.g., Richstone et al. 1998). These two facts alone suggest that binary SMBHs should be commonplace. Of course, one or both of the SMBHs in a binary will only be detectable as quasars when they are actively accreting. One of the leading proposed mechanisms to trigger strong accretion (quasar) activity is galaxy mergers (e.g., Hernquist 1989, Kauffmann & Haehnelt 2000, Hopkins et al. 2008, and references therein), so merging galaxies with binary quasars should also be common. Begelman et al. (1980) first discussed binary SMBH evolution, from galaxy merger to coalescence, as an explanation for the form and motion of radio jets in active galactic nuclei (AGNs). The “final parsec problem” (Milosavljević & Merritt 2003)—whether the coalescence of a binary SMBH ultimately stalls (Milosavljević & Merritt 2001), proceeds to rapid coalescence (e.g., Escala et al. 2004), or instead recoils or is ejected (e.g., Madau & Quataert 2004)—has important implications for the detection

of gravitational waves and for the spin and demography of SMBHs.

In a broader context, astronomers hypothesize that “feedback”—whereby dynamical interactions between galaxies trigger accretion onto their SMBHs—mediates the tight correlation between galaxy central black hole masses and the velocity dispersions σ_* of galaxy bulges ($M_{\text{BH}} - \sigma_*$; Ferrarese et al. 2000; Gebhardt et al. 2000). The resulting quasars grow in the galaxy cores until they blow out the very galactic gas that feeds them (e.g., Granato et al. 2004), choking off star formation, and eventually leading to passive elliptical galaxies (Hopkins et al. 2007; Kormendy et al. 2009). This feedback paradigm dovetails with cosmological models of hierarchical structure formation if quasar activity is induced by massive mergers (e.g., Wyithe & Loeb 2002, 2005). Major mergers (i.e., those with mass ratios above ~ 0.3 ; Shen 2009) between gas-rich galaxies most efficiently channel large quantities of gas inward, fostering starbursts and feeding rapid black hole growth. Deep high-resolution imaging of quasar host galaxies (Bahcall et al. 1997; Guyon et al. 2006; Bennert et al. 2008) shows strong evidence for fine structure and tidal tails expected from past gravitational interactions. Radio-quiet quasar hosts tend to be found in gas-rich galaxy mergers that form intermediate-mass galaxies, while radio-loud QSOs reside in massive early-type galaxies, most of which also show signs of recent mergers or interactions (Wolf & Sheinis 2008). The far-infrared (FIR) emission of QSOs appears to follow a merger-driven evolution from FIR-bright to FIR-faint QSOs (Veilleux et al. 2009a).

⁶ Visiting Astronomer, Kitt Peak National Observatory and Cerro Tololo Inter-American Observatory, National Optical Astronomy Observatory, which is operated by the Association of Universities for Research in Astronomy, Inc. (AURA) under cooperative agreement with the National Science Foundation.

The measured excess of quasars with $\lesssim 40$ kpc separations (e.g., Hennawi et al. 2006; Myers et al. 2007, 2008) over the extrapolated large-scale quasar correlation function may indeed be due to mutual triggering, but is also debated to arise naturally from their locally overdense environments (Hopkins et al. 2008). The dynamics and timescales of major mergers are therefore of the utmost interest.

To date, the merger hypothesis is supported by findings of spatially resolved binary AGNs in just a handful of $z < 0.1$ galaxies with one or both of the nuclei heavily obscured in X-rays (NGC 6240, Komossa et al. 2003; Arp 299, Zezas et al. 2003; Mrk 463, Bianchi et al. 2008), by the unusual BL Lac-type object OJ 287 (Sillanpaa et al. 1988; Valtonen et al. 2009), and perhaps by X-shaped morphology in radio galaxies (e.g., Merritt & Ekers 2002; Liu 2004; Cheung 2007). In addition, COSMOS J100043.15+020637.2 is known to contain two AGNs resolved at $0''.5$ (~ 1.8 kpc) separation in *HST*/ACS imaging, which have a radial velocity difference of $\Delta v = 150 \text{ km s}^{-1}$, and appear to be hosted by a galaxy with a tidal tail (Comerford et al. 2009a).

Interest in spatially unresolved systems (spectroscopic binary AGN candidates) has surged of late, spawned largely from the troves of Sloan Digital Sky Survey (SDSS) spectroscopy. The unusual system SDSS J153636.22+1044127.0 (Boroson & Lauer 2009) has a spectrum with two broad-line systems separated by $\Delta v = 3500 \text{ km s}^{-1}$, and also has a nearby radio (Wrobel & Laor 2009) and optical (Decarli et al. 2009) counterpart. The physical nature of this system has been heavily debated (e.g., Chornock et al. 2010; Lauer & Boroson 2009; Tang & Grindlay 2009), largely because spatially unresolved quasars with double-peaked broad emission lines are a quite common phenomenon (e.g., Strateva et al. 2003). Another spatially unresolved system, SDSS J092712.65+294344.0, shows two broad and one narrow emission-line systems in its spectrum, with $\Delta v = 2650 \text{ km s}^{-1}$, sparking discussion about whether it is a chance superposition (Shields et al. 2009), hosts a recoiling SMBH (Komossa et al. 2008b), or is a bound binary SMBH inside a single narrow-line region (Bogdanović et al. 2009; Dotti et al. 2009). Quasars with double-peaked narrow emission lines are relatively common (e.g., there are at least 167 such systems in the SDSS; Liu et al. 2009). From the DEEP2 Galaxy Redshift Survey, Comerford et al. (2009b) found that more than a third of type 2 AGN show [O III] line velocities significantly ($50\text{--}300 \text{ km s}^{-1}$) offset from the redshifts of the host galaxies' stars, arguing that the most likely explanation is inspiralling SMBHs in merger-remnant galaxies. Smith et al. (2009) find that about 1% of (21,592) quasars in SDSS DR7 have detectable double-peaked [O III] emission-line profiles. Only two of those appear to be spatially resolved, but the (single-fiber spectroscopy) sample selection is strongly biased against nuclei with separations greater than about an arcsecond.

Spatially unresolved systems such as these are relatively easy to find in large spectroscopic samples. However, because of the lack of spatial information, the velocity offsets are open to a variety of interpretations depending on the relative strength and velocity of narrow and/or broad emission-line systems: small-scale gas kinematics, asymmetric or thermally inhomogeneous accretion disks, AGN outflows or jets, recoiling or orbiting SMBHs, or disturbed or rotating narrow-line regions (Smith et al. 2009). Furthermore, spectroscopic samples are biased against binary AGNs that are very close in redshift (i.e., unresolved in velocity space), or those that are more widely separated on the sky. For instance, in the SDSS spectroscopic

survey, the fiber diameter is $3''$, and the minimum separation of fibers on a plate is $55''$ on the sky. So, except in rare cases with multiple overlapping spectroscopic plates, any binary quasar with separation in between these two values could only be found from dedicated follow-up spectroscopy.

Why are spatially resolved active nuclei in mergers so rare? First, they may be heavily shrouded and therefore only detectable as ultraluminous infrared galaxies (ULIRGs). ULIRGs have bolometric luminosities rivalling quasars, and by some (*Hubble Space Telescope* (*HST*) *I*-band) estimates, as many as 40% retain double active nuclei (Cui et al. 2001). A binary fraction in local ULIRGs of at least 40% is also consistent with *R*- and *K*-band ground-based data obtained under $\lesssim 1''$ seeing and later confirmed with *H*-band *HST* data (Veilleux et al. 2002, 2006). Among dust-reddened quasars, Urrutia et al. (2008) found that 85% show evidence of merging in images of their host galaxies. Second, detectable mergers may be rare simply because the lifetime of the resolvable-but-unmerged interacting phase is extremely short (Mortlock et al. 1999; Foreman et al. 2009). Third, gas-rich major mergers should trace quasars, and therefore should mainly have occurred near the “quasar epoch” at higher redshifts ($z \gtrsim 1.5$; e.g., Khochfar & Burkert 2001; Wolf et al. 2003; Silverman et al. 2005), where detection of extended host galaxy light is challenging.

The prevailing view in the literature (e.g., Djorgovski 1991; Kochanek et al. 1999; Mortlock et al. 1999; Myers et al. 2007) is that the excess of quasars with small (< 40 kpc) separations is evidence for nuclear triggering in galaxies during dissipative mergers. According to Hopkins et al. (2007), the excess measured clustering (e.g., Hennawi et al. 2006; Myers et al. 2007, 2008) indeed represents compelling evidence for the merger-driven origin of quasars. However, they also note that attaching all quasars to moderately rich dark matter environments in which mergers are most likely to occur is sufficient to explain the observed excess of binary quasars at < 40 kpc, even if they are not triggering each other in a bound orbit. That is, they just happen to be neighbors where the typical observed velocity differences could represent $\sim \text{Mpc}$ separations along the line of sight rather than dynamical velocities, and their properties should be statistically indistinguishable from those of single quasars. The discovery of binary quasars whose hosts are clearly interacting thus presents rare opportunities to study what merging/triggering really looks like, and allows for derivation of important quantities associated with the interaction.

In Section 2, we discuss the discovery of SDSS J1254+0846, a pair of luminous quasars with nearly identical redshift, hosted by a galaxy merger. Unique among known spatially resolved systems, SDSS J1254+0846, is at a scale that suggests it is an *ongoing* merger rather than a relaxed or remnant system. SDSS J1254+0846 can thus be used to help study boundary conditions for gas-rich galaxy mergers. The description and results of our deep follow-up multiwavelength imaging and spectroscopy follow in Section 3, including estimates of the black hole masses and Eddington ratios. To verify the plausibility of the merger scenario and determine if it is possible to infer any properties of the interaction, we compare numerical *N*-body simulations to the observed properties of the system in Section 4. In Section 5, we consider the hypothesis that the pair might be lensed, which we find to be extremely unlikely. We present our conclusions in Section 6. Throughout, we assume the following cosmological parameters for distance-dependent quantities: $\Omega_m = 0.3$, $\Omega_\Lambda = 0.7$, and $H_0 = 72 \text{ km s}^{-1} \text{ Mpc}^{-1}$,

which yields an angular size scale of $5.5 \text{ kpc arcsec}^{-1}$ at the redshift of our system ($z \sim 0.44$).

2. DISCOVERY OF SDSS J1254+0846

The objects SDSS J125455.09+084653.9 (SDSS J1254+0846 A hereafter) and SDSS J125454.87+084652.1 (SDSS J1254+0846 B hereafter) were targeted as a pair (SDSS J1254+0846 hereafter) as part of a complete sample of binary quasar candidates with small transverse separations drawn from SDSS DR6 photometry (A. D. Myers et al. 2010, in preparation). A preliminary targeted follow-up campaign of such objects (for DR4) is discussed in Myers et al. (2008). Quasar candidates were selected as having $g < 20.85$ and either the “ultraviolet excess (UVX) quasar” and/or “low-redshift quasar” Bayesian classification flags set in the catalog of Richards et al. (2009).⁷ These cuts ensure a high efficiency of quasar pairs in the targets and a reasonably homogeneous sample over redshifts of $0.4 < z < 2.4$. Pairs of quasar candidates were then followed up spectroscopically if they had an angular separation of $3''$ – $6''$. To extend the completeness of the sample as a function of comoving separation, the sample was also extended to pairs with separations of $6''$ – $\sim 7''.7$, if neither component had a known redshift at $z > 1.2$.

Following an extensive observational campaign with the Ritchey–Chrétien (R–C) spectrograph on the Mayall 4 m at Kitt Peak National Observatory and the double spectrograph on the 200 inch (5 m) Hale Telescope at Palomar Observatory, the sample of target quasar pairs from which SDSS J1254+0846 was drawn is now complete (again, see A. D. Myers et al. 2010, in preparation). SDSS J1254+0846 itself was discovered to be a binary quasar on the night of 2008 February 11 and confirmed as such on 2008 February 12 at Kitt Peak (Myers and Hennawi observing). As was the case for all candidate binary quasars observed on that run, a $1''.5$ by $204''$ long-slit set at the position angle of SDSS J1254+0846 was used, allowing both components to be simultaneously observed. The KPC-10A grating was used yielding a resolution of $\sim 5 \text{ \AA}$ and a wavelength coverage of ~ 3800 – 7800 \AA . As the seeing was $\sim 1''.5$ on the nights in question, and the component separation of SDSS J1254+0846 is $3''.8$, care was taken when reducing the data to prevent the component spectra from merging. The component spectra were reduced iteratively using *xid1*’s low-redshift package (Hennawi, Burles, Schlegel, & Prochaska; <http://www.ucolick.org/~xavier/LowRedux/>) with the procedure guided by hand using a boxcar extraction to ensure no overlap of the spectra.

At 1.4 GHz, the host and its quasars are undetected, with flux less than 2.5 mJy at a resolution of $45''$ (250 kpc) in the NRAO VLA Sky Survey (NVSS; Condon et al. 1998) and less than 1 mJy at a resolution of $5''$ (28 kpc) in the FIRST survey (White et al. 1997). Following Ivezić et al. (2002), combining the 1 mJy upper limit with the *i*-band magnitudes of the quasars, both components are radio quiet.

As the sample of binary quasar candidates from which it was drawn is now complete, SDSS J1254+0846 should be unremarkable. On the other hand, it is the lowest redshift binary quasar currently known and it has an unusually low χ^2 color similarity statistic (see Hennawi et al. 2006; Myers et al. 2008) of 0.2, meaning that the colors of its two components are practically identical. Across all five bands, their SDSS (PSF) magnitudes differ by 2.28 ± 0.08 (flux ratio 8.27 ± 0.61), identical within

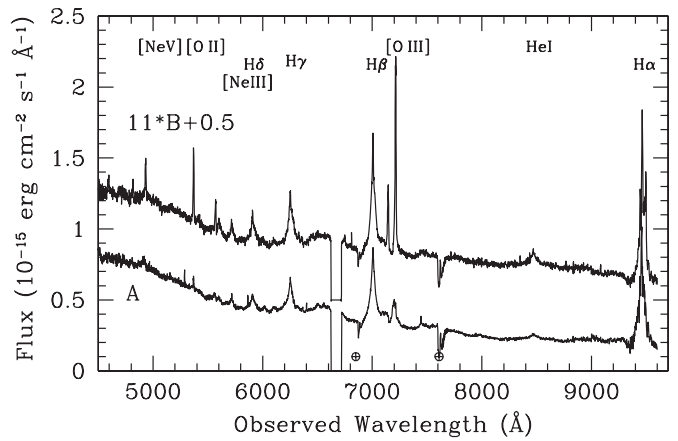


Figure 1. Optical spectra. The two components’ spectra are plotted from 4500 to 9600 Å, with the B component scaled up and shifted for clarity. Despite the factor of ~ 11 difference in flux normalization, the redshift, continuum, and broad-line shapes are all remarkably similar. The most striking difference is in the equivalent widths of the narrow emission lines; all the forbidden lines of [Ne V], [O II], and [O III] are relatively much stronger in B. Major emission-line species are labeled along the top. Major atmospheric absorption bands are marked with circumscribed crosses along the bottom. CCD gaps are evident in both spectra between ~ 6600 and 6700 \AA .

the errors. Based on the $(g - i)$ versus redshift (Green et al. 2009) for SDSS quasars, the optical colors of these quasars are marginally (~ 0.2 mag) blue relative to the mean, but consistent with those expected at this redshift. The striking feature of SDSS J1254+0846 was discovered as we imaged this pair and several others in our *Chandra*/NOAO joint program (PI: P. Green; *Chandra* ObsID 10315) to observed binary quasars and their environments. Images we obtained on the nights of 2009 March 18 at NOAO’s Kitt Peak Observatory with the MOSAIC imager on the 4 m Mayall Telescope (Barkhouse and Myers observing) immediately revealed bright tidal tails emanating from the quasar pair. The uniqueness of the system led us to procure further deep imaging and spectroscopy at other facilities.

3. OBSERVATIONS

3.1. Optical Spectroscopy

We obtained deeper spectroscopy of both quasars on 2009 May 22 simultaneously through a single $0''.9$ slit in seeing of $\sim 0''.4$ using the IMACS spectrograph on the Baade–Magellan Telescope at the Las Campanas Observatory in Chile. We centered the slit on QSO B, at a position angle of 61° to include QSO A. We used the $f/2$ camera mode with a 300 lines mm^{-1} grism, giving a wavelength range of ~ 4000 – 9600 \AA and a dispersion of $1.34 \text{ \AA pixel}^{-1}$. We combined four exposures of 1200 s each, and flux-calibrated using the original SDSS spectrum, except for $> 9200 \text{ \AA}$ where we used the standard star LTT 3864, rescaled to match the SDSS spectrum, in the overlap region 8900–9050 Å.

Figure 1 overlays the two spectra, with the B component scaled up and shifted for clarity. Despite the factor of ~ 11 difference in flux normalization, the redshift, continuum, and broad-line shapes are all remarkably similar. The continuum ratio varies from about 11 near 5000 Å to about 10 near 8200 Å (observed frame). The discrepancy of 20%–30% between flux ratios in our IMACS spectroscopy and the SDSS imaging $8.27 (\pm 0.61)$ could be due to variability of either QSO component between the two epochs. This is consistent with the somewhat larger

⁷ `uvxts=1` or `lowzts=1`.

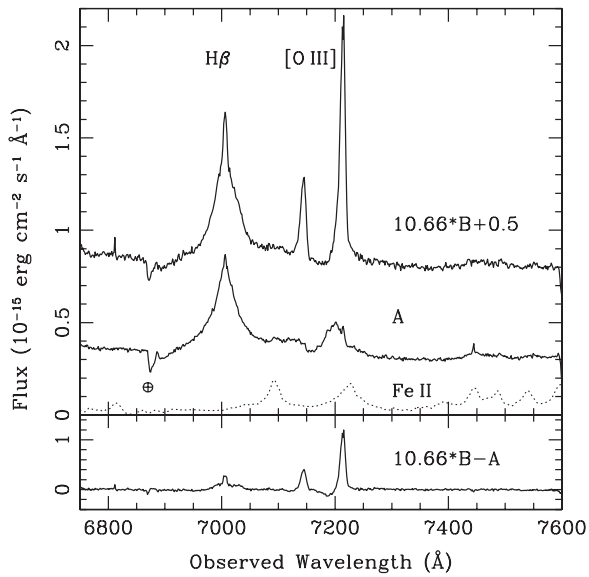


Figure 2. Optical spectral features near $H\beta$. In the upper panel, the two components’ spectra are plotted from 6750 to 7600 Å, with the B component scaled up and shifted for clarity. The dashed curve is the (arbitrarily scaled) optical Fe II emission template of I Zw 1 (Boroson & Green 1992). Such iron multiplet emission appears to represent at best a minor contribution to either spectrum. The residual of $10.66*B - A$ is shown in the bottom panel. The flat residuals highlight the similarity of the redshifts, continuum shape, and broad-line profiles. The apparent trough blueward of the stronger [O III] line is due to the broader, blueshifted profile of the line in A.

discrepancy in the blue, since QSO variability is known to increase toward shorter wavelengths (e.g., Wilhite et al. 2005). Some of the difference could also be due to slit position and alignment.

The most striking difference is in the equivalent widths of the narrow emission lines. All the forbidden lines of [Ne V], [O II], and [O III] are *relatively* much stronger in B (larger equivalent widths). To test whether the spectrum we have extracted for QSO B is contaminated by scattered light from A, we extracted a spectrum on the other side of QSO A at a distance equal to the separation of A from B. No significant spectral features are detectable, so we conclude that contamination of the B spectrum by scattered light from A is negligible.

Figures 2 and 3 highlight the regions around $H\beta$ and $H\delta$, respectively. The A spectrum looks somewhat smoother because of its higher signal-to-noise ratio (S/N). The residuals plotted in the lower panels, from simple scaled subtraction with no velocity shift, are direct evidence that the redshifts of the two quasars are virtually identical. Separate cross-correlations of the two spectra against the SDSS median composite quasar spectrum using IRAF xcsao (Kurtz et al. 1992), and excluding telluric line regions and CCD artifacts yield $z_A = 0.43919 \pm 0.00028$ ($R = 10.5^8$) and $z_B = 0.440095 \pm 0.00011$ ($R = 15.0$). From direct cross-correlation of the A and B spectra we find a velocity offset for A–B of $-215 \pm 100 \text{ km s}^{-1}$ ($R = 6.7$), consistent with essentially no significant velocity difference.

The residuals in Figures 2 and 3 also illustrate that the most significant differences between the spectra are in the narrow-line components. However, some differences are also evident in the broad-line regions (BLRs). The spectroscopic differences effectively preclude an interpretation of the pair as possibly lensed (see Section 5 for further discussion). Although it is

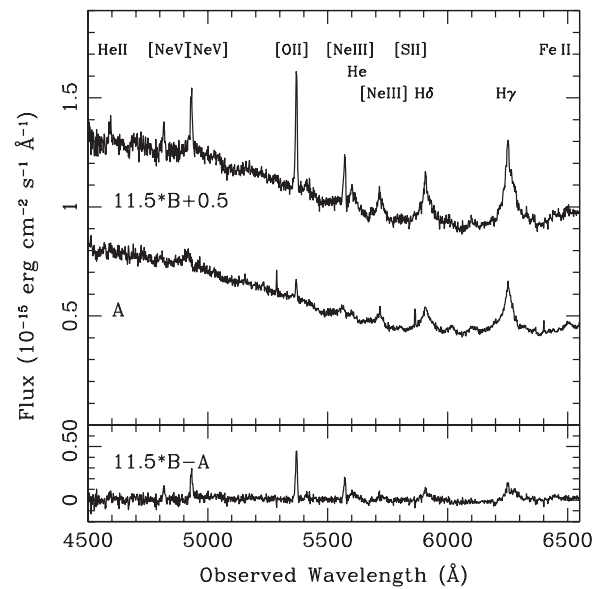


Figure 3. Optical spectral features near $H\gamma$. In the upper panel, the two components’ spectra are plotted from 4500 to 6500 Å, with the B component scaled up and shifted for clarity. The residual of $11.5*B - A$ is shown in the bottom panel.

difficult to tell from plots of this rescaled format, the A/B luminosity ratio is much smaller between the two components in low-ionization forbidden lines (ratio 1.6 ± 0.2 in the [O II] emission line) than in their continuum emission. While the [O II] emission cannot be assumed to be a pure indicator of star formation rate in the presence of an AGN (Yan et al. 2006), a larger fraction of [O II] emission should arise from star formation in the host galaxy, so the smaller A/B ratio is evidence that the two nuclei probably share a host.

We note that if these nuclei were spatially unresolved but with the same velocity difference and flux ratios, the system would not be detected in a spectroscopic SDSS search for binary quasars such as that of Smith et al. (2009). Direct addition of the two components’ spectra (as if in a single aperture) results in a rather normal-looking quasar spectrum—the B component is easily subsumed in the A spectrum, merely highlighting the very peaks of the narrow lines. On the other hand, if the tiny velocity difference is due to the serendipitously small angle of our sight line along the orbital axis, then a different projection would increase the observed velocity difference, as would a bound system with smaller physical separation between the nuclei.

3.2. Optical Imaging

On the same night, 2009 May 22, at the Baade–Magellan Telescope, we obtained 20 minutes of imaging (four exposures of 300 s) in both Sloan r and i bands. The IMACS $f/2$ camera has $0''.2$ pixels, and the seeing was $0''.4$. We subtracted the CCD bias level and flattened the field response using averaged dome projector flat images in each filter as usual. Images were then co-added with the SWarp package (Bertin 2006; ver. 2.17.6), and object detection and measurement were made with SExtractor (Bertin & Arnouts 1996). Photometric calibration was performed using dereddened magnitudes from SDSS DR7 for matching objects in the field.⁹ The r -band image in Figure 4 shows the two bright nuclei of SDSS J1254+0846 and two symmetrical tidal tails spanning some 75 kpc at the quasar redshift.

⁸ R is the ratio of the correlation peak to the amplitude of the asymmetric noise.

⁹ We compare SDSS `model_Mag` to SExtractor `MAG_AUTO` values.

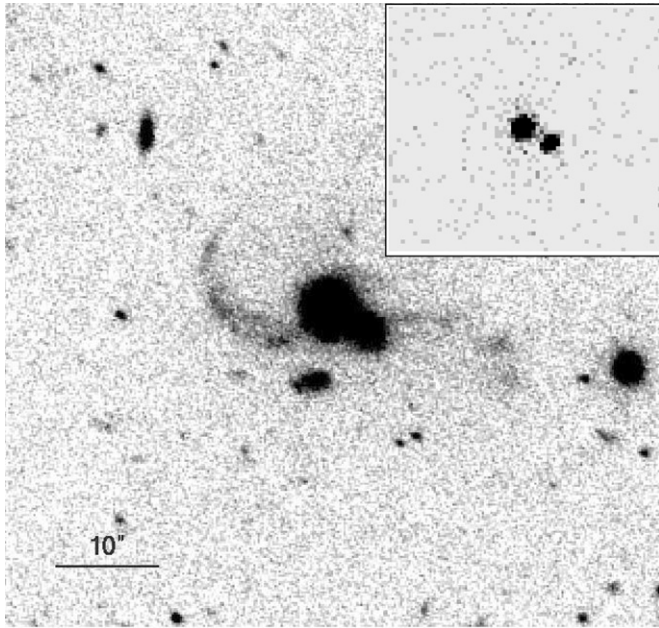


Figure 4. Optical and X-ray images of SDSS J1254+0846. This optical image ($1'$ on a side, N up, E to the left) is the median of four five-minute exposures obtained on 2009 May 22 in $1''$ seeing with an r -band filter on the IMACS camera at the Magellan/Baade Telescope at the Las Campanas Observatory in Chile. The two bright quasar nuclei are evident. The brighter A component ($r = 17.5$) was identified spectroscopically in the SDSS as a quasar. Discovery spectroscopy of the B component ($r = 19.2$) was obtained as part of our binary quasar survey. This follow-up IMACS image clearly reveals the tidal arms of a host galaxy merger. Inset: our *Chandra* 16 ks ACIS-S X-ray image (same scale and orientation, but $0'.5$ on a side) shows the two nuclei, which have both typical f_X/f_{opt} and power-law spectral slopes (Green et al. 2009). There is no evidence for extended emission as might be expected from a host (or lensing-mass) group or cluster.

3.3. *Chandra* X-ray Observations

We obtained X-ray images of the quasar pair with the *Chandra* X-ray Observatory on 2009 February 23 at the ACIS-S aim point for 16 ksec. The X-ray components are well-resolved by *Chandra*, and correspond closely ($<0'.2$) to their SDSS counterparts. To avoid cross-contamination, we extracted the X-ray photons from apertures corresponding to 90% of the counts (for 1.5 keV). The NE (SW) components yield 1869 (381) net counts, respectively, in the 0.5–8 keV range. We fit an X-ray power-law spectral model,

$$N(E) = A E^{-\Gamma} \times \exp \left[-N_H^{\text{Gal}} \sigma(E) - N_H^z \sigma(E(1+z_{\text{abs}})) \right],$$

to the counts using the CIAO tool *Sherpa*, where A is the normalization in photons $\text{cm}^2 \text{s}^{-1} \text{keV}^{-1}$ and $\sigma(E)$ is the absorption cross section (Morrison & McCammon 1983; Wilms et al. 2000). We fix N_H^{Gal} at the appropriate Galactic neutral absorbing column 1.9×10^{20} atoms cm^{-2} , and include an intrinsic absorber with the neutral column N_H^z at the source redshift. We group counts to a minimum of 16 per bin and fit using the χ^2 statistic with variance computed from the data. The best-fit model for both components is $\Gamma = 2.0$ (with 90% confidence uncertainties of 0.05 and 0.2 for the NE/SW components, respectively), and only upper limits to any intrinsic absorption ($N_H^{\text{intr}} < 2.7$ and 7.2×10^{20} atoms cm^{-2} , respectively). These values are quite typical of SDSS quasars (Green et al. 2009). The 2 keV A/B flux ratio is 4.9, somewhat less than the optical flux ratio. The X-ray-to-optical ratio is often param-

eterized by the X-ray-to-optical spectral slope α_{ox} ,¹⁰ which is 1.41 for A and 1.37 for B. X-rays in quasars become weaker relative to optical emission as luminosity increases, and both these quasars fall along the expected trends (Steffen et al. 2006; Green et al. 2009). Statistical tests have shown that the correlation is weaker with redshift, so that the $\alpha_{\text{ox}}(L)$ relationship is not a secondary effect of quasar evolution combined with the strong $L-z$ trends of flux-limited quasar samples. While anecdotal, SDSS J1254+0846 confirms in a single system that the observed α_{ox} trend with luminosity in quasars is followed even by quasars at the same epoch and in the same large-scale environment. Both members of the pair are slightly X-ray bright for their estimated UV (2500 Å) luminosity. Our images suggest that the merger is essentially face-on between massive disk galaxies that are close to coplanar. If the quasar accretion disks are reasonably well aligned with their galactic host disks,¹¹ then our sight line may simply avoid the extinction and reddening associated with a large angle to the line of sight.

3.4. Radio Observations

We observed SDSS J1254+0846 with the VLA near transit on UT 2009 September 25 and 27, with net exposure times of 2350 s and 7053 s, respectively, using the DnC configuration under NRAO proposal code AG826. We chose center frequency 8.4601 GHz (8.5 GHz hereafter) with a bandwidth of 100 MHz for each circular polarization. Observations were phase-referenced to the calibrator J1254+1141 whose positional accuracy was less than 2 mas. The switching angle was 3° and the switching time was 240 s. Observations of 3C 286 were used to set the amplitude scale to an accuracy of about 3%. The data were calibrated using the 2009 December 31 release of the NRAO AIPS software. Each day's visibility data for SDSS J1254+0846 were concatenated and the AIPS task *imagr* was used to form and deconvolve a Stokes I image. Natural weighting was used to optimize sensitivity, giving an angular resolution at FWHM of $9'.4$ times $7'.2$ elongated at the position angle -29° . One source was detected and an elliptical-Gaussian fit to it, yielding the following integrated flux density, position, and one-dimensional position error: $S = 0.26 \pm 0.03$ mJy, $\alpha(J2000) = 12^{\text{h}}54^{\text{m}}55^{\text{s}}.08$, $\delta(J2000) = +08^\circ46'53''.9$, and $\sigma_{\text{VLA}} = 0'.3$. The flux density error is the quadratic sum of the 3% scale error and the fit residual. The position error is the quadratic sum of a term due to the phase-calibrator position error (less than $0''.002$), the phase-referencing strategies (estimated to be $0'.1$), and the S/N ($0'.3$). The source was unresolved and, given the modest S/N data, the corresponding diameter is less than the geometric-mean beam width, $8'.2$.

The 8.5 GHz emission from SDSS J1254+0846 has a radio luminosity, $L_R = \nu L_\nu$, of 1.5×10^{40} erg s^{-1} and is unresolved, with a diameter of less than $8'.2$ (45 kpc). This scale encompasses the inner portions of the host galaxy merger, plus quasars A and B. Higher-resolution imaging using the Expanded VLA (Perley et al. 2009) is needed to localize the emission from each quasar. In the interim, we note that our *Chandra* data on quasars A and B implies a 0.2–20 keV luminosity L_X of 7.9×10^{44} erg s^{-1} . Laor & Behar (2008) propose that both active stars and radio-quiet AGNs owe their radio emission to similar coronal processes, following $L_R/L_X \sim 10^{-5}$, where $L_R = \nu L_\nu$ at 5 GHz. For a

¹⁰ α_{ox} is the slope of a hypothetical power law from 2500 Å to 2 keV; $\alpha_{\text{ox}} = 0.3838 \log(l_{2500\text{Å}}/l_{2\text{keV}})$.

¹¹ In radio galaxies, there is some general evidence against such an alignment (Schmitt et al. 2002).

spectral slope of -0.5 (Kellermann et al. 1994), the observed 8.5 GHz luminosity corresponds to 1.1×10^{40} erg s $^{-1}$ at 5 GHz. Thus $L_R/L_X \sim 1.4 \times 10^{-5}$, just the ratio expected for the radio-quiet quasars A and B. This simple, testable argument suggests that the 8.5 GHz emission arises from both quasars A and B, without substantial contribution from the extended host galaxy.

3.5. Black Hole Mass and Eddington Ratio

Given our high-quality spectra, we can estimate the black hole mass and Eddington ratios for each quasar. Most AGN black hole mass estimators derive from reverberation mapping (Peterson 1993; Wandel et al. 1999), whereby time delays τ between continuum and broad emission-line variations are used to deduce the size of the BLR. For single-epoch optical spectra, the continuum luminosity $L_\lambda(5100 \text{ \AA})$ can be used as a surrogate for the BLR radius R (Koratkar & Gaskell 1991; Kaspi et al. 2000, 2005). By combining τ with the emission-line width (most directly using $H\beta$), a virial mass for the black hole can be estimated (e.g., Vestergaard & Peterson 2006).

We use the `sp1ot` task within IRAF to deblend narrow and broad $H\beta$ above the continuum in each quasar spectrum, and we correct our $H\beta$ line width measurements for spectral resolution and narrow-line contamination following Peterson et al. (2004). For quasar A, we measure a $H\beta$ FWHM of 2904 ± 200 km s $^{-1}$. The log of the continuum luminosity at 5100 Å is 45.422 in erg s $^{-1}$. If we assume the bolometric correction of 9.26 for 5100 Å luminosity from Richards et al. (2006), then $\log L_{\text{Bol}} = 46.39$. For quasar B, we measure a $H\beta$ FWHM of 2782 ± 200 km s $^{-1}$. The continuum luminosity at 5100 Å is 44.394 erg s $^{-1}$ so $\log L_{\text{Bol}} = 45.36$.

From McLure & Dunlop (2004), we adopt the black hole mass estimator

$$\log \left(\frac{M_{\text{BH, vir}}}{M_\odot} \right) = 0.672 + 0.61 \log \left(\frac{\lambda L_\lambda}{10^{44} \text{ erg s}^{-1}} \right) + 2 \log \left(\frac{\text{FWHM}}{\text{km s}^{-1}} \right). \quad (1)$$

We thereby estimate black hole masses for quasars A and B such that $\log(\frac{M_{\text{BH, vir}}}{M_\odot}) = 8.46$ and 7.80, respectively. We estimate uncertainties of about 0.4 dex based on Vestergaard & Peterson (2006).

The Eddington luminosity, assuming a composition of pure hydrogen, is given by

$$L_{\text{Edd}} = \frac{4\pi G M_{\text{BH}} m_p c}{\sigma_T} = 1.26 \times 10^{38} \left(\frac{M_{\text{BH}}}{M_\odot} \right) \text{ erg s}^{-1}, \quad (2)$$

where M_{BH} is the mass of the black hole, m_p is the proton mass, and σ_T is the Thompson scattering cross section. Therefore, we find the Eddington ratios $L_{\text{Bol}}/L_{\text{Edd}}$ for quasars A and B to be 0.67 and 0.29, respectively. Comparing to Shen et al. (2008) for SDSS quasars in similar ranges of redshift and L_{Bol} (see their Figure 12), the Eddington ratio for quasar B is just 0.6 σ above the mean in $\log L_{\text{Bol}}/L_{\text{Edd}}$, whereas for A the ratio is $\approx 3\sigma$ high. This could be evidence that accretion rates are strongly boosted during close interactions among massive merging galaxies.

4. MERGER SIMULATIONS

We can further understand the properties of SDSS J1254+0846 via numerical simulations. Galaxy mergers may be a significant triggering mechanism for quasar activity, and there is

growing interest in verifying and understanding this connection more completely. Since the majority of theoretical models (see, e.g., Wyithe & Loeb 2003; Volonteri et al. 2003; Hopkins et al. 2008) associate the most active phase of evolution (and thus most of the black hole growth) with nuclear coalescence, most quasars are expected to be hosted by systems where many of the telltale signs of interaction (disturbed morphology, tidal bridges, and tails) no longer exist, or are difficult to find underneath the glare of the quasar. In many cases, deep imaging at high spatial resolution (Dunlop et al. 2003) but also high S/N (e.g., Bennert et al. 2008) is required to find evidence for these faint structures.

In this context, SDSS J1254+0846, a pre-coalescence merger with two observed quasars, provides a unique opportunity to probe the early phases of the proposed merger/triggering mechanism. One of the most powerful insights into this system is via numerical simulation, i.e., designing numerical models of the current system that can be evolved, modified, and compared to the observed system. We have undertaken just such a task using numerical techniques that are extensively detailed in the existing literature (e.g., Springel et al. 2005; Cox et al. 2006; Hopkins et al. 2008; Jonsson et al. 2009). Briefly, initial equilibrium disk models are constructed to be representative of disks at the appropriate redshift. These models are then initialized on a prograde orbit and allowed to evolve using the N -body/SPH code Gadget (Springel 2010) from a distant separation, through their interaction, to their eventual merger. The references provided above include extensive descriptions of these models, and their generic outcome.

A representative result of such a numerical modeling experiment is shown in Figure 5, which displays a prograde parabolic galaxy merger with baryonic mass ratio 2:1, viewed after the second close passage, but prior to the final coalescence. This model was selected owing to both its nuclear separation and the position and extent of the tidal features showing a remarkable resemblance to SDSS J1254+0846. On the other hand, the black hole masses are off by a factor of ~ 2 and their accretion rates by a factor of 5–10.

Determining a suitable match proved to be a time-consuming endeavor which required the analysis of ~ 200 merger simulations to isolated the orbits and orientations that best reproduce the observed tidal features, and the simulation of eight additional mergers to perfect this match. In general, the symmetric tidal features place a relatively tight constraint on the relative orientation of the disk spins to that of the orbital plane. Specifically, the spin-orbit orientation is required to be less than $\sim 30^\circ$. Furthermore, the relationship between the tidal features and the nuclear separation demanded a relatively large impact parameter ($R_{\text{peri}} \sim 4 R_{\text{disk}}$) such that it had a wide first passage, and a glancing second passage, prior to the final coalescence. Additional velocity information for both the nuclei and the tails would place even tighter constraints on these parameters.

The observed tidal features offer a direct means to constrain the orbital parameters. However, the set of observed galaxy properties—specifically the accreting black holes—provide insufficient information to uniquely determine the properties of the interacting galaxies. The matching experiment here only informs us that the progenitor spiral galaxies are required to be sufficiently large (i.e., scale length of the stellar disk $R_{\text{disk}} \gtrsim 4$ kpc), to produce the length of the tidal tails, and that they must have contained pre-existing stellar bulges to match the black hole masses observed at this early merger stage. It might be possible to quantify the properties of the progenitors better with additional information about the observed system or using

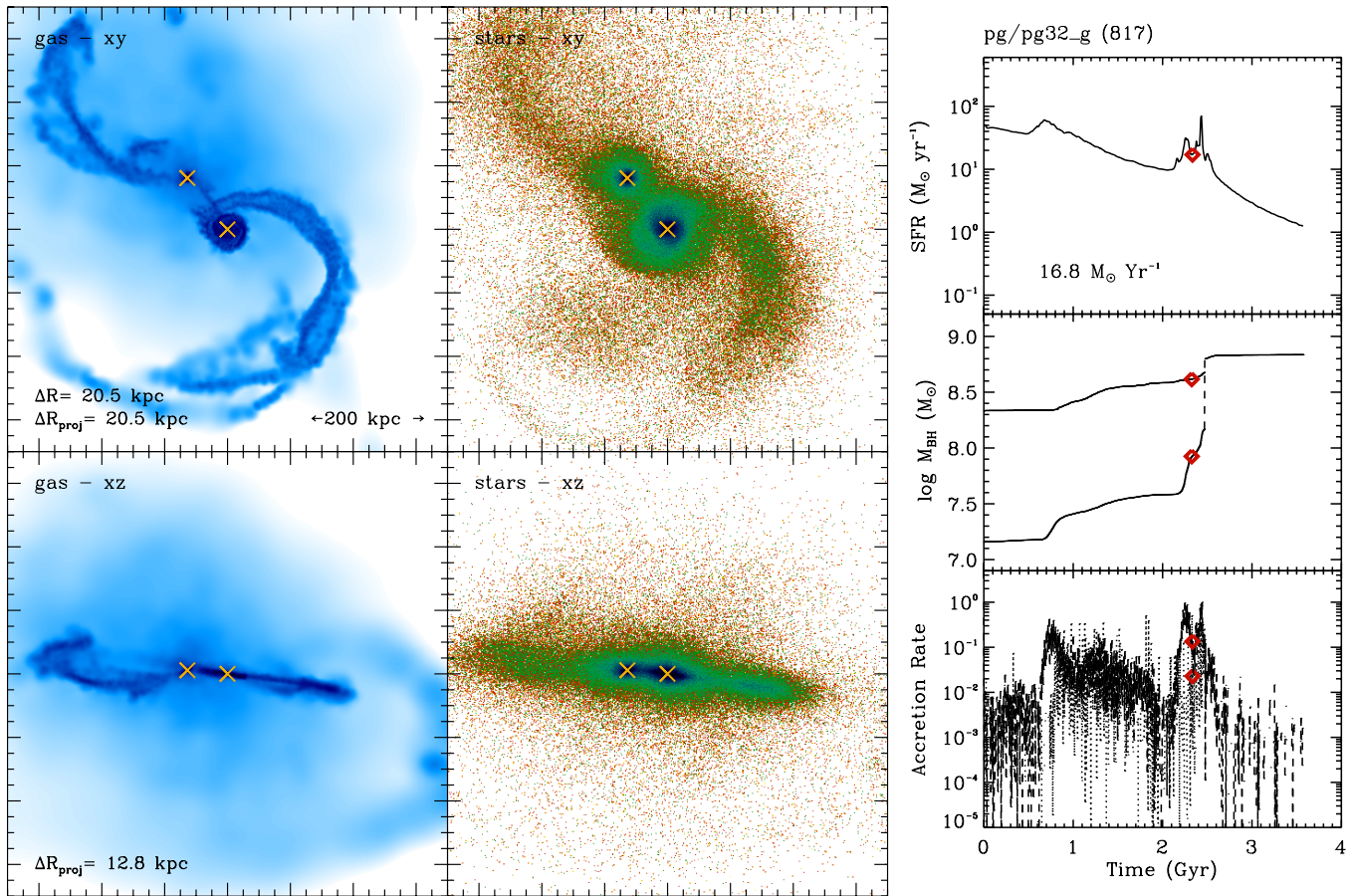


Figure 5. Numerical simulation of a merger like SDSS J1254+0846. The left panels show the gas distribution, and the middle panels the stars in the xy and xz planes, for this model of a prograde merger of two massive disks. The right panels show the model star formation rates, nuclear black hole masses, and accretion rates for the two components. The epoch displayed in the images at left, 2.3 Gyr, is marked with red diamonds in the plots to the right, at which the nuclear separation, the position and extent of the tidal features (in the xy plane), the black hole masses, and their accretion rates resemble those of SDSS J1254+0846.

additional models, but we caution that the predicted black hole properties include assumptions about the initial disk model, including the seed black hole masses, as well as black hole accretion that occurs well below our model resolution, and thus additional model-matching is unwarranted until a larger sample of observed galaxies exists. In particular, we should not expect (indeed, we should be skeptical of) a perfect match between the observed and model-predicted accretion rate onto the SMBHs (and thus also the luminosity of the quasars at any given time), because stochastic (unpredictable) accretion events appear to turn ignite nuclear accretion activity at any given time along the merger sequence in ULIRGs (e.g., Veilleux et al. 2009b). The lower right panel of Figure 5 makes clear how noisy the accretion is expected to be.

Given the success of our search for a model that matches many of the properties of the observed system, it is fair to ask what we learn from such an experiment. First, we have provided additional evidence that galaxy mergers are a plausible scenario for triggering quasar activity. In fact, nearly all quantities are extracted from the matched model. The orbit, the orientation, and the progenitor galaxies are fully consistent with, and even expected in, a merger-triggered scenario for quasar formation. Second, we have identified a case where the progenitor galaxies participating in the galaxy merger contain massive bulges and, hence, SMBHs. While most theoretical models do not currently make testable predictions about the abundance of such systems during the hierarchical growth of galaxies and black holes, a

larger sample of such observed systems will certainly motivate additional investigation.

5. A GRAVITATIONAL LENS?

Given the identical redshift, similar colors, and the strong similarities in the continuum slope and broad-line profiles between components A and B, is it possible that the pair is lensed? It seems highly unlikely for several reasons. First, the observed optical spectra are very different, whereas gravitational lensing should be essentially achromatic. Second, the A/B flux ratio is unusually large for a lensed system. Third, to achieve the rather wide A/B separation, a massive lens is expected at intermediate redshift, which should be sufficiently luminous as to be evident in the images. Fourth, an intervening lens galaxy should produce some absorption signature in the quasar spectra. We discuss these four objections to a lens interpretation in turn.

Spectral differences between quasar image components are common even in bona fide lenses (e.g., Wisotzki et al. 1993; Burud et al. 2002a, 2002b; Oguri et al. 2005; Sluse et al. 2007). These differences are typically explained as the effect of either microlensing, or as light path time delays sampling intrinsic quasar spectral variability. Even with macrolensing only, anisotropy in the source may create spectroscopic differences along the slightly different sight lines (Green 2006; Perna & Keeton 2009). While particularly illuminating of source structure, such effects are expected to be much more subtle than

those observed here. If the pair is indeed lensed, then microlensing remains the most likely explanation for the spectral differences. However, microlensing-induced spectroscopic differences should primarily affect emission from the more compact emission regions of the source quasar—the continuum, or perhaps the broad lines. The observed spectroscopic differences are instead predominantly in the narrow lines, whose emission region is too large (hundreds to thousands of parsecs; e.g., Motta et al. 2004; Bennert et al. 2002) to be affected by microlensing.

Let us consider the second objection to a lens interpretation, the unusually large A/B flux ratio in SDSS J1254+0846. While most known bona fide lens components indeed show smaller flux ratios, this is quite possibly a selection effect caused by flux-limited surveys from which lens candidates are found. Furthermore, if the system were indeed lensed and microlensing were indeed the cause of the spectroscopic differences described above, the unmicro- (but still macro-) lensed flux ratio would not likely be that observed in the broadband photometry. Since microlensing is *least* likely to affect the narrow-line region, the flux ratio of the narrow lines might more accurately represent the true macrolensed flux ratio. The A/B ratio of [O III] line flux above the continuum is only about 5.8 ± 0.4 . For comparison, the mean/median/mode of the A/B *I*-band (HST F814W) image flux ratio for 60 lensed quasars in the CASTLES¹² database (E. Falco 2010, private communication) is 5.4/2.6/1.5, but 8 of the 60 (13%) have ratios above 9. Therefore, the large observed image flux ratio in SDSS J1254+0846 does not on its own rule out a lens interpretation.

The third objection is that a luminous lensing galaxy is expected to be visible. One possibility is that the lensing galaxy of this system happens to be the tidally disturbed system visible in our images. One can ask post-facto, how likely is it to find an interacting pair of massive spirals with spectacular tidal arms, well-centered near the mean position of the quasar images? If the spin of a galaxy is randomly aligned with the orbit, then only 1/6th of the time is it aligned within 30° of the orbital spin, and so only 1/36th of the time would both be aligned, such as needed to produce the observed tails. It is difficult—perhaps fruitless—to attempt a further probability calculation for such an alignment, given the huge parent sample in which this exceedingly rare object was found, the complex selection effects, and the lack of imaging and spectroscopy of comparable depths in large statistical samples. Clearly the most definitive test of the hypothesis of a tidally disturbed lens galaxy would be deep spectroscopy of the faint tails to determine the redshift of the associated stellar population.

To further investigate the lens hypothesis, we have run lens models using GRAVLENS software (Keeton 2001)¹³ for a singular isothermal sphere (henceforth SIS) at all intervening redshifts. For the observed total flux ratio of ~ 9 , we find reasonable velocity dispersions near 300 km s^{-1} for $0.15 < z_{\text{lens}} < 0.3$. From the *I*-band Tully–Fisher relation (Masters et al. 2006), we expect a $\sigma_v = 300 \text{ km s}^{-1}$ galaxy to have absolute *I*-band magnitude -20.8 ± 0.2 . For a redshift $z \sim 0.22$, the expected SDSS *i*-band magnitude for such a galaxy is about 19.5, which is about the same as the fainter quasar. The expected position of the center of mass of the lens is determined in the model by the observed flux ratio. Larger A/B flux ratio means

proportionally *smaller* distance from the lens to component A. In the Appendix, we have attempted to subtract the A and B nuclear point sources and determine the location, brightness, and significance of any galaxy light between them. In summary, while there is some evidence for extended emission around the quasar nuclei themselves, we find no evidence for significant extended emission with a centroid consistent with the expected lensing galaxy position.

Fourth, a lensing galaxy might be expected to produce detectable signatures in the quasar spectrum. We find insufficient contribution from stellar emission (either from a $z = 0.44$ host or from a putative intervening lensing galaxy) to create any detectable spectral features. For an absorber at a plausible $z_{\text{lens}} = 0.22$, the more commonly detected optical/UV intervening absorption lines (such as Ly α or the Mg II doublet near 2800 Å rest) are in the UV. Detection of the Ca II $\lambda\lambda 3934, 3969$ Å (*H* and *K*) or Na I D $\lambda\lambda 5891, 5897$ absorption would be feasible, but since these are extremely rare (Wild & Hewett 2005), a non-detection here is not useful. Detailed inspection of the spectra of both A and B components yields no evidence for any significant absorption lines that might suggest an intervening (lensing) galaxy.

X-rays sample intervening gas and dust in all phases. Our X-ray spectral fit, including a $z_{\text{lens}} = 0.22$ absorption component, yields an upper limit of $2.2 \times 10^{20} \text{ atoms cm}^{-2}$ from the A component spectrum for an unchanged best-fit continuum slope $\Gamma = 2.01 \pm 0.08$. The absorption upper limit from B is about three times weaker.

On balance, we have considered several significant objections to a lensing scenario, and we believe that despite the nearly identical redshifts, SDSS J1254+0846 A and B truly represent a binary quasar. Our simulations confirm what by all appearances is a merger with orbits fortuitously close to the plane of the sky, for which the very similar observed nuclear velocities are much more likely.

6. CONCLUSIONS

The quasars SDSS J125455.09+084653.9 (A) and SDSS J125454.87+084652.1 (B) are within 21 kpc projected transverse separation at their common redshift of $z = 0.44$, hosted by a galaxy merger showing clear tidal tail features. The quasar A/B flux ratio is nearly constant across all five SDSS bands, and they show a remarkably small $\sim 2\sigma$ velocity difference of $\sim 200 \text{ km s}^{-1}$. We find especially strong differences between their narrow emission-line equivalent widths, and their Eddington ratios. The spectroscopic features of A—in particular, weak [O III]5007] with evidence for a blueshifted component—are associated with high accretion rates (Aoki et al. 2005; Komossa et al. 2008a) and outflows. We suggest that A is very strongly accreting. Given its weak, blueshifted [O III], it would be a candidate for a broad absorption line (BAL) quasar, verifiable with UV spectroscopy of the C IV region. A counterargument is that it has a normal X-ray/optical flux ratio, which is rare in BAL quasars (Green et al. 2001; Gallagher et al. 2006).

The close coincidence of the positions, colors, and redshifts of the two quasar components raises the suspicion of lensing. We examine a variety of counterarguments, most prominently the strong optical spectroscopic emission-line differences, but also the large image flux ratio, and the absence of either emission or absorption signatures from an intervening lens galaxy. Deep spectroscopy of the tidal tails should prove interesting for a test of the lens model, but also for more detailed study of

¹² CfA-Arizona Space Telescope Lens Survey information is hosted at <http://www.cfa.harvard.edu/castles>.

¹³ Software available at <http://redfiv.rutgers.edu/~keeton/gravlens/>.

the stellar populations in this unique system. Although each counterargument to lensing may have known caveats, we find the overall evidence to be quite persuasive that the pair is indeed a binary quasar. Perhaps the strongest argument is simply the association of a binary quasar with a clear merger of two massive disk galaxies. While expected under the merger hypothesis for quasar triggering, we deem the coincidence of such a system with a lensing configuration to be exceedingly unlikely.

Indeed, a simple explanation for the very similar nuclear radial velocities, as suggested by the galaxy images and numerical simulations, is that the merger is apparently along an orbit close to the plane of the sky. SDSS J1254+0846 may represent a rare system where the orientations of accretion disks in the quasar nuclei can be constrained by the system configuration as being close to our line of sight (modulo the unknown relative orientations between accretion disks and galaxy disks). Such an orientation would be consistent with the unobscured, type 1 spectroscopic nature of both quasars.

There are strong advantages to studying spatially resolved binary quasars (SRBQs) such as these. SRBQs can be particularly useful when chosen from well-defined parent samples. First, such samples probe *ongoing* mergers. Second, the spatial and velocity information, especially when combined with well-resolved spectra providing separate black hole mass estimates, offers more constraints on the properties of the merging components and the evolution of the merger. We have found a good match via numerical merger simulations for the orbit, the orientation, and the galaxies in this system, showing that it is fully consistent with a merger-triggered scenario for quasar formation, where the progenitor galaxies already contain massive bulges. By selection, SRBQs are likely to be face-on, which makes them ideal for providing *morphological* constraints on merger models via, e.g., follow-up with *HST* or ground-based adaptive optics. The use of uniform SRBQ parent samples further allows us to place these systems in their larger cosmological context, which is crucial if we are to understand the role of merger-triggered SMBH accretion, and its relationship with galaxy evolution.

Support for this work was provided by the National Aeronautics and Space Administration through *Chandra* Award Number GO9-0114A issued by the *Chandra* X-ray Observatory Center, which is operated by the Smithsonian Astrophysical Observatory for and on behalf of the National Aeronautics Space Administration under contract NAS8-03060. This paper includes data gathered with the 6.5 m Magellan Telescopes located at Las Campanas Observatory, Chile. Discovery optical images were obtained at Kitt Peak National Observatory, National Optical Astronomy Observatory, which is operated by the Association of Universities for Research in Astronomy (AURA) under cooperative agreement with the National Science Foundation. This research has made use of data obtained from the *Chandra* Data Archive and software provided by the *Chandra* X-ray Center (CXC) in the application packages CIAO and Sherpa. This paper has used data from the SDSS archive. Funding for the SDSS and SDSS-II has been provided by the Alfred P. Sloan Foundation, the Participating Institutions, the NSF, the US Department of Energy, the National Aeronautics and Space Administration (NASA), the Japanese Monbukagakusho, the Max Planck Society, and the Higher Education Funding Council for England. The SDSS Web site is at <http://www.sdss.org/>. Thanks to Emilio Falco for valuable discussions.

Facilities: Mayall, Magellan:Baade, CXO, VLA

APPENDIX

SURFACE PHOTOMETRY

We used the two-dimensional galaxy-image fitting program GALFIT (Peng et al. 2002) to decompose the quasar and host-galaxy light of image components A and B and to detect and fit underlying extended features. GALFIT can simultaneously fit one or more objects in an image choosing from a library of functional forms (e.g., exponential, etc.; Sérsic 1968; de Vaucouleurs 1948). For convolution with the point-spread function (PSF) of the telescope optics, we first created PSF stars from stars within the image close to the location of the quasars. Most stars either had too few counts, especially in the PSF wings, or were saturated. We thus created an artificial Gaussian profile with an FWHM corresponding to that of non-saturated stars observed in the image. Qualitatively, the results are the same as using real star images, with the advantage of zero noise in the artificial PSF image. We find that $\gtrsim 95\%$ of flux is removed when we fit stars in the frame, with the residuals due primarily to ellipticity in the observed PSF.

For both the r and the i filters, we subtracted the sky background and fitted two PSFs at the locations of quasars A and B. Simultaneously, we fitted and subtracted closely neighboring and bright objects. Due to the saturation of quasar A in our images, we fixed the flux ratio of the PSFs of quasars A and B to the ratio given in SDSS-DR7 (using “psfMag_r;” “psfMag_i”). We used the SDSS PSF magnitude for quasar B also to calibrate our results. Then, we fitted the host galaxies of quasar A and quasar B and a potential underlying lensing galaxy with either a de Vaucouleurs (1948) profile or the more general Sérsic (1968) profile:

$$\Sigma(r) = \Sigma_{\text{eff}} \exp \left[-\kappa_n \left(\left(\frac{r}{r_{\text{eff}}} \right)^{1/n} - 1 \right) \right] \quad (\text{A1})$$

where Σ_{eff} is the pixel surface brightness at the effective radius r_{eff} , and n is the Sérsic index. In this generalized form, an exponential disk profile has $n = 1$, and a de Vaucouleurs (1948) profile has $n = 4$. In general, fitting a Sérsic (1968) profile gives more flexibility to the fit, but also adds an additional free parameter to an already complicated fit, which can result in an unphysically large Sérsic index or an unphysically small effective radius. For this reason, we decided to fix the Sérsic index to either 4 or 1 (depending on the resulting χ^2) and set the minimum allowed effective radius to 3 pixels (i.e., the minimum resolvable size given by the FWHM). We then chose the best fit based on the residuals and χ^2 statistics. Note that we also constructed masks to exclude tidal structures during the fitting procedure; however, the effect of the latter on the results is negligible.

In addition to fitting quasar A and quasar B with the PSF model, we followed these four approaches: (1) we fitted one “joint” host galaxy at a (starting) location in between quasars A and B; (2) we fitted two host galaxies at the locations of quasars A and B; (3) we fitted two host galaxies at the locations of quasars A and B plus another galaxy (“lens”) fixed at a position along the A – B line expected from a SIS lens model¹⁴; (4) we fitted two host galaxies at the location of quasars A and B plus another galaxy (“lens”) close to the location of quasar A.

¹⁴ More precisely, at the location along the line between quasars A and B where the ratio of separations (quasar B – lens)/(quasar A – lens) equals the A/B flux ratio based on the SDSS PSF magnitudes.

Table 1
Results from GALFIT Fitting

Filter	PSF Quasar A (mag)	PSF Quasar B (mag)	Host Quasar A (mag)	Host Quasar B (mag)	Lens (mag)
(1)	(2)	(3)	(4)	(5)	(6)
<i>r</i>	17.15	19.50	17.52	19.33	...
	17.15	19.50	17.98	19.33	18.23
<i>i</i>	17.07	19.36	18.44	19.85	...
	17.07	19.36	18.75	19.49	18.37

Notes. GALFIT host galaxy fit results. Column 1: filter: SDSS *r* or SDSS *i*. Column 2: SDSS PSF magnitude of quasar A. Column 3: SDSS PSF magnitude of quasar B. Column 4: best-fit magnitude of quasar A host galaxy. Column 5: best-fit magnitude of quasar B host galaxy. Column 6: best-fit magnitude of third “lens” galaxy close to A.

Only models 2 and 4 yield acceptable fits, with four slightly preferred by comparison of the reduced χ^2 (i.e., taking into account the larger number of parameters in model 4). Although it is easier to “hide” a lens galaxy near component A as in model 4, the lens model predicts that the brighter image (“A”) is outside of the Einstein radius and is further from the lens. The fainter image is closer to the lens and is interior to the Einstein radius. Therefore, one result of our experiments is that host galaxies are required for both A and B. A single “joint” host is unacceptable: GALFIT instead preferred a host galaxy at the location of either A or B. The second result is that a third extended component (a putative “lens” galaxy in addition to host galaxies for A and B) is preferred by the fits, but the best-fit position is not the one predicted by a simple SIS lens model. Fixing an additional de Vaucouleurs (1948) profile closer to the fainter quasar results in an unphysically tiny effective radius. Freeing the coordinates results in a second extended component (in addition to the host galaxy) at the location of quasar B, and one of the two components becomes either unphysically huge or vanishingly small. The third (“lens”) galaxy is allowed only if it is much closer to quasar A. In Table 1, we summarize the results in both *r* and *i* filters for the best-fit models, based on residuals and χ^2 statistics. Based on our experience with fitting quasar host galaxies (and simulations carried out; Bennert et al. 2010; see also Kim et al. 2008), we conservatively estimate the uncertainties of the AGN luminosity to 0.2 mag and those of the host galaxies to 0.5 mag.

Note that fitting this system is complicated and our results have to be interpreted with caution. In general, the decomposition of complex images in multiple components is a difficult statistical challenge due to the degeneracies involved, and the highly nonlinear dependence of the likelihood on a large number of parameters. Decomposing quasar and host-galaxy light is already difficult. Here, the fitting is further complicated by the fact that we have two quasars close to each other, one of which is saturated, with possibly a merging host galaxy and/or tidal disturbances and/or another underlying galaxy. Keeping in mind these cautionary notes, we can conclude the following: there seem to be two host galaxies at the location of quasars A and B, not just a relaxed galaxy hosting two quasars. While there is no evidence for another galaxy close to the location of quasar B, we cannot exclude the presence of another galaxy close to the location of quasar A. However, based on the flux ratios of QSOs A and B, we would expect the lensing galaxy to fall closer to QSO B. Thus, our modeling rules out significant extended emission with a centroid that is consistent with the expected lensing galaxy position. Deep images of higher S/N and smaller PSF

are warranted, either from *HST* or using adaptive optics from the ground.

REFERENCES

- Aoki, K., Kawaguchi, T., & Ohta, K. 2005, *ApJ*, **618**, 601
- Bahcall, J. N., Kirhakos, S., Saxe, D. H., & Schneider, D. P. 1997, *ApJ*, **479**, 642
- Begelman, M. C., Blandford, R. D., & Rees, M. J. 1980, *Nature*, **287**, 307
- Bennert, N., Canalizo, G., Jungwiert, B., Stockton, A., Schweizer, F., Peng, C. Y., & Lacy, M. 2008, *ApJ*, **677**, 846
- Bennert, N., Falcke, H., Schulz, H., Wilson, A. S., & Wills, B. J. 2002, *ApJ*, **574**, L105
- Bennert, V. N., Treu, T., Woo, J.-H., Malkan, M. A., Le Bris, A., Auger, M. W., Gallagher, S., & Blandford, R. D. 2010, *ApJ*, **708**, 1507
- Bertin, E. 2006, SWarp Version 2.16 User’s Guide (Paris: Terapix), <http://terapix.iap.fr/IMG/pdf/swarp.pdf>
- Bertin, E., & Arnouts, S. 1996, *A&AS*, **117**, 393
- Bianchi, S., Chiaberge, M., Piconcelli, E., Guainazzi, M., & Matt, G. 2008, *MNRAS*, **386**, 105
- Bogdanović, T., Eracleous, M., & Sigurdsson, S. 2009, *ApJ*, **697**, 288
- Boroson, T. A., & Green, R. F. 1992, *ApJS*, **80**, 109
- Boroson, T. A., & Lauer, T. R. 2009, *Nature*, **458**, 53
- Burud, I., et al. 2002a, *A&A*, **383**, 71
- Burud, I., et al. 2002b, *A&A*, **391**, 481
- Cheung, C. C. 2007, *AJ*, **133**, 2097
- Chornock, R., et al. 2010, *ApJ*, **709**, L39
- Comerford, J. M., Griffith, R. L., Gerke, B. F., Cooper, M. C., Newman, J. A., Davis, M., & Stern, D. 2009a, *ApJ*, **702**, L82
- Comerford, J. M., et al. 2009b, *ApJ*, **698**, 956
- Condon, J. J., Cotton, W. D., Greisen, E. W., Yin, Q. F., Perley, R. A., Taylor, G. B., & Broderick, J. J. 1998, *AJ*, **115**, 1693
- Cox, T. J., Dutta, S. N., Di Matteo, T., Hernquist, L., Hopkins, P. F., Robertson, B., & Springel, V. 2006, *ApJ*, **650**, 791
- Cui, J., et al. 2001, *AJ*, **122**, 63
- Decarli, R., Dotti, M., Falomo, R., Treves, A., Colpi, M., Kotilainen, J. K., Montouri, C., & Uslenghi, M. 2009, *ApJ*, **703**, L76
- de Vaucouleurs, G. 1948, *Ann. d’Astrophys.*, **11**, 247
- Djorgovski, S. 1991, in ASP Conf. Ser. 21, The Space Distribution of Quasars, ed. D. Crampton (San Francisco, CA: ASP), **349**
- Dotti, M., Montouri, C., Decarli, R., Volonteri, M., Colpi, M., & Haardt, F. 2009, *MNRAS*, **398**, L73
- Dunlop, J. S., McLure, R. J., Kukula, M. J., Baum, S. A., O’Dea, C. P., & Hughes, D. H. 2003, *MNRAS*, **340**, 1095
- Escala, A., Larson, R. B., Coppi, P. S., & Mardones, D. 2004, *ApJ*, **607**, 765
- Ferrarese, L., & Merritt, D. 2000, *ApJ*, **539**, L9
- Foreman, G., Volonteri, M., & Dotti, M. 2009, *ApJ*, **693**, 1554
- Gallagher, S. C., Brandt, W. N., Chartas, G., Priddey, R., Garmire, G. P., & Sambruna, R. M. 2006, *ApJ*, **644**, 709
- Gebhardt, K., et al. 2000, *ApJ*, **539**, L13
- Granato, G. L., et al. 2004, *ApJ*, **600**, 580
- Green, P. J. 2006, *ApJ*, **644**, 733
- Green, P. J., Aldcroft, T. L., Mathur, S., Wilkes, B. J., & Elvis, M. 2001, *ApJ*, **558**, 109
- Green, P. J., et al. 2009, *ApJ*, **690**, 644
- Guyon, O., Sanders, D. B., & Stockton, A. 2006, *ApJS*, **166**, 89
- Hennawi, J. F., et al. 2006, *AJ*, **131**, 1
- Hernquist, L. 1989, *Nature*, **340**, 687
- Hopkins, P. F., Hernquist, L., Cox, T. J., & Kereš, D. 2008, *ApJS*, **175**, 356
- Hopkins, P. F., et al. 2007, *ApJ*, **662**, 110
- Ivezić, Z., et al. 2002, *AJ*, **124**, 2364
- Jonsson, P., Groves, B., & Cox, T. J. 2009, arXiv:0906.2156
- Kaspi, S., Maoz, D., Netzer, H., Peterson, B. M., Vestergaard, M., & Jannuzi, B. T. 2005, *ApJ*, **629**, 61
- Kaspi, S., Smith, P. S., Netzer, H., Maoz, D., Jannuzi, B. T., & Giveon, U. 2000, *ApJ*, **533**, 631
- Kauffmann, G., & Haehnelt, M. 2000, *MNRAS*, **311**, 576
- Keeton, C. R. 2001, arXiv:astro-ph/0102340
- Kellermann, K. I., Sramek, R. A., Schmidt, M., Green, R. F., & Shaffer, D. B. 1994, *AJ*, **108**, 1163
- Kim, M., Ho, L. C., Peng, C. Y., Barth, A. J., & Im, M. 2008, *ApJS*, **179**, 283
- Khochfar, S., & Burkert, A. 2001, *ApJ*, **561**, 517
- Kochanek, C. S., Falco, E., & Munoz, J. A. 1999, *ApJ*, **510**, 590
- Komossa, S., Xu, D., Zhou, H., Storchi-Bergmann, T., & Binette, L. 2008a, *ApJ*, **680**, 926
- Komossa, S., Zhou, H., & Lu, H. 2008b, *ApJ*, **678**, L81

- Komossa, S., et al. 2003, *ApJ*, **582**, L15
- Koratkar, A. P., & Gaskell, C. M. 1991, *ApJ*, **370**, L61
- Kormendy, J., Fisher, D. B., Cornell, M. E., & Bender, R. 2009, *ApJS*, **182**, 216
- Kurtz, M. J., Mink, D. J., Wyatt, W. F., Fabricant, D. G., Torres, G., Kriss, G. A., & Tonry, J. L. 1992, in ASP Conf. Ser. 25, *Astronomical Data Analysis Software and Systems I*, ed. D. M. Worrall, C. Biemesderfer, & J. Barnes (San Francisco, CA: ASP), 432
- Laor, A., & Behar, E. 2008, *MNRAS*, **390**, 847
- Lauer, T. R., & Boroson, T. A. 2009, *ApJ*, **703**, 930
- Liu, F. K. 2004, *MNRAS*, **347**, 1357
- Liu, X., Shen, Y., Strauss, M. A., & Greene, J. E. 2009, arXiv:0908.2426
- Madau, P., & Quataert, E. 2004, *ApJ*, **606**, L17
- Masters, K. L., Springob, C. M., Haynes, M. P., & Giovanelli, R. 2006, *ApJ*, **653**, 861
- McLure, R. J., & Dunlop, J. S. 2004, *MNRAS*, **352**, 1390
- Merritt, D., & Ekers, R. D. 2002, *Science*, **297**, 1310
- Milosavljević, M., & Merritt, D. 2001, *ApJ*, **563**, 34
- Milosavljević, M., & Merritt, D. 2003, in AIP Conf. Proc. 686, *The Astrophysics of Gravitational Wave Sources* (Melville, NY: AIP), 201
- Morrison, R., & McCammon, D. 1983, *ApJ*, **270**, 119
- Mortlock, D. J., Webster, R. L., & Francis, P. J. 1999, *MNRAS*, **309**, 836
- Motta, V., Mediavilla, E., Muñoz, J. A., & Falco, E. 2004, *ApJ*, **613**, 86
- Myers, A. D., et al. 2007, *ApJ*, **658**, 99
- Myers, A. D., Richards, G. T., Brunner, R. J., Schneider, D. P., Strand, N. E., Hall, P. B., Blomquist, J. A., & York, D. G. 2008, *ApJ*, **678**, 635
- Oguri, M., et al. 2005, *ApJ*, **622**, 106
- Peng, C. Y., Ho, L. C., Impey, C. D., & Rix, H.-W. 2002, *AJ*, **124**, 266
- Perley, R., et al. 2009, *Proc. IEEE*, **97**, 1448
- Perna, R., & Keeton, C. R. 2009, *MNRAS*, **397**, 1084
- Peterson, B. M. 1993, *PASP*, **105**, 247
- Peterson, B. M., et al. 2004, *ApJ*, **613**, 682
- Richards, G. T., et al. 2006, *ApJS*, **166**, 470
- Richards, G. T., et al. 2009, *ApJS*, **180**, 67
- Richstone, D., et al. 1998, *Nature*, **395**, A14
- Schmitt, H. R., Pringle, J. E., Clarke, C. J., & Kinney, A. L. 2002, *ApJ*, **575**, 150
- Sérsic, J. L. 1968, *Atlas de Galaxias Australes* (Cordoba: Observatorio Astronómico)
- Shen, Y. 2009, *ApJ*, **704**, 89
- Shen, Y., Greene, J. E., Strauss, M. A., Richards, G. T., & Schneider, D. P. 2008, *ApJ*, **680**, 169
- Shields, G. A., Bonning, E. W., & Salviander, S. 2009, *ApJ*, **696**, 1367
- Sillanpää, A., Haarala, S., Valtonen, M. J., Sundelius, B., & Byrd, G. G. 1988, *ApJ*, **325**, 628
- Silverman, J. D., et al. 2005, *ApJ*, **624**, 630
- Sluse, D., Claeskens, J.-F., Hutsemékers, D., & Surdej, J. 2007, *A&A*, **468**, 885
- Smith, K. L., Shields, G. A., Bonning, E. W., McMullen, C. C., & Salviander, S. 2009, arXiv:0908.1998
- Springel, V. 2010, *MNRAS*, **401**, 791
- Springel, V., Di Matteo, T., & Hernquist, L. 2005, *MNRAS*, **361**, 776
- Steffen, A. T., Strateva, I., Brandt, W. N., Alexander, D. M., Koekemoer, A. M., Lehmer, B. D., Schneider, D. P., & Vignali, C. 2006, *AJ*, **131**, 2826
- Strateva, I. V., et al. 2003, *AJ*, **126**, 1720
- Tang, S., & Grindlay, J. 2009, *ApJ*, **704**, 1189
- Toomre, A., & Toomre, J. 1972, *ApJ*, **178**, 623
- Urrutia, T., Lacy, M., & Becker, R. H. 2008, *ApJ*, **674**, 80
- Valtonen, M. J., et al. 2009, *ApJ*, **698**, 781
- Veilleux, S., Kim, D.-C., & Sanders, D. B. 2002, *ApJS*, **143**, 315
- Veilleux, S., et al. 2006, *ApJ*, **643**, 707
- Veilleux, S., et al. 2009a, *ApJ*, **701**, 587
- Veilleux, S., et al. 2009b, *ApJS*, **182**, 628
- Vestergaard, M., & Peterson, B. M. 2006, *ApJ*, **641**, 689
- Volonteri, M., Haardt, F., & Madau, P. 2003, *ApJ*, **582**, 559
- Wandel, A., Peterson, B. M., & Malkan, M. A. 1999, *ApJ*, **526**, 579
- White, R. L., Becker, R. H., Helfand, D. J., & Gregg, M. D. 1997, *ApJ*, **475**, 479 (<http://sundog.stsci.edu/top.html>)
- Wild, V., & Hewett, P. C. 2005, *MNRAS*, **361**, L30
- Wilhite, B. C., Vanden Berk, D. E., Kron, R. G., Schneider, D. P., Pereyra, N., Brunner, R. J., Richards, G. T., & Brinkmann, J. V. 2005, *ApJ*, **633**, 638
- Wilms, J., Allen, A., & McCray, R. 2000, *ApJ*, **542**, 914
- Wisotzki, L., Koehler, T., Kayser, R., & Reimers, D. 1993, *A&A*, **278**, L15
- Wolf, C., et al. 2003, *A&A*, **408**, 499
- Wolf, M. J., & Sheinis, A. I. 2008, *AJ*, **136**, 1587
- Wrobel, J. M., & Laor, A. 2009, *ApJ*, **699**, L22
- Wyithe, J. S. B., & Loeb, A. 2002, *ApJ*, **581**, 886
- Wyithe, J. S. B., & Loeb, A. 2003, *ApJ*, **595**, 614
- Wyithe, J. S. B., & Loeb, A. 2005, *ApJ*, **634**, 910
- Yan, R., Newman, J. A., Faber, S. M., Konidaris, N., Koo, D., & Davis, M. 2006, *ApJ*, **648**, 281
- Zezas, A., Ward, M. J., & Murray, S. S. 2003, *ApJ*, **594**, L31